RESEARCH ARTICLE

On BESS Allocation in AC/DC Networks Using a Sensitivities-Based Loss Model Combined With Injection Shift Factors

LUIS M. CASTRO[ID]

Faculty of Engineering, Department of Electrical Energy, National Autonomous University of Mexico (UNAM), Mexico City 04510, Mexico

e-mail: luismcastro@fi-b.unam.mx

ABSTRACT The operation of AC/DC networks formed by voltage source converters (VSC) is difficult to optimize. In particular, the minimization of transmission losses is a challenging task to address because several VSC-coupled AC grids interact simultaneously to supply the load. In this context, this article presents a practical approach for power loss minimization in hybrid networks by allocating battery energy storage systems (BESS). The crux of this method is a sensitivities-based loss model combined with power injection shift factors. One that suitably exploits the topological structure and fundamental parameters of the hybrid network. The most suitable nodes for the BESS connection can be straightforwardly identified by using this method, while reducing the power losses and improving the system operating efficiency. Multi-terminal AC/DC networks of arbitrary topology can be studied with this new approach, considering converters with grid-following, grid-forming, fixed-power control strategies, and converters interfacing systems with no local generation or with renewable plants only. The section of case studies includes two multi-period power system analyses. One to confirm the effectiveness of the method and another to showcase its practicality, using four-terminal and six-terminal VSC-based AC/DC networks with complex patterns of demand, wind speed and solar irradiance of the renewable sources.

INDEX TERMS AC/DC networks, battery energy storage systems, injection shift factors, power loss minimization, renewable plants, voltage source converters.

I. INTRODUCTION

Electrical networks are evolving with startlingly rapid progress. This is the case for the interconnection of neighboring systems through DC-based transmission links formed by voltage source converters (VSC), contrary to the use of classical AC tie lines [1]. The resulting AC/DC networks, together with the integration of renewable plants, give rise to new operating challenges that await solutions [2]. Despite this, system operators strive to guarantee continuous and efficient electrical service while preserving system security. Modernizing electrical networks with cutting-edge technology is a must to achieve these goals. A case in point is the use of battery energy storage systems (BESS), which can make the system more efficient from technical and economic point of view [3]. Due to its flexibility to provide auxiliary services, the BESS can be successfully used to alleviate a wide variety of operating problems if properly placed in the system [4]. This is also true for the allocation of BESS in overly complex VSC-based AC/DC grids, representing an open research problem that requires a practical approach to its solution.

BESS allocation in power grids can pursue a wide variety of objectives, often related to auxiliary services at the distribution and transmission levels. To this end, recent studies have focused on improving the voltage stability in weak grids [5], primary power reserves for frequency control [6], [7], power oscillation damping [8], and combined

The associate editor coordinating the review of this manuscript and approving it for publication was Ning Kang[ID].

minimization of generation costs and load shedding costs [9]. However, the installation of BESS can also be driven by the massive incorporation of renewable sources, such as photovoltaic (PV) plants, while pursuing the minimization of the system losses. Examples of this can be found in the literature where the energy-time shift strategy of batteries [10] and the duck curve phenomenon of PV plants [11] have also been studied to complement the related optimization analyzes. With similar objectives in mind, the BESS allocation with PV plants has been conducted considering the response to the system demand and the reduction of the deviations of system voltage [12], renewable generation with uncertainty [13], [14], and the mitigation of problems related to power quality [15]. Certainly, minimizing power losses by placing BESS in distribution networks is a direct objective pursued in these types of studies [16], [17]. One that can also be indirectly achieved by minimizing nodal voltage deviations [17], [18], or by using loss sensitivity indices [19]. Similarly, multistep hierarchical frameworks have been developed to reduce voltage violations and system operation costs aided by optimal BESS allocation [20], [21].

1) SCOPE AND JUSTIFICATION OF THE PROPOSED APPROACH

From the above, it follows that most methods aim to reduce system losses explicitly or implicitly by minimizing operation costs or nodal voltage deviations. More importantly, BESS allocation has only concentrated on classical AC power grids. In contrast, this work presents a practical approach for the minimization of power losses by BESS allocation in AC/DC networks formed by VSC units with standard control strategies. Its hallmark is a comprehensive sensitivities-based power loss model suitably combined with power injection shift factors (ISF). Changes in power loss, either negative or positive, can be quantified as a function of the power injected by the charging and discharging operations of the BESS. Thus, the most suitable nodes for BESS allocation that minimize the AC/DC power losses can be directly identified.

While the use of BESS in distribution networks is a cost-effective solution to mitigate power fluctuations caused by renewable sources or to reduce short-term demand spikes, its application to high-voltage VSC-based AC/DC networks may not be so obvious. But recent advances in the design and capacity of batteries have prompted operating schemes that can positively impact bulk transmission systems such as electric energy time shift, peak shaving, and renewable energy time shift. Due to its operating flexibility, grid-connected BESS can simultaneously provide secondary services in power networks such as reactive power regulation and spinning reserve. Therefore, the optimum BESS allocation in AC/DC power networks is advantageous for system operation, not only in terms of efficiency (reduction of power losses) but also for participating in key ancillary services. Regarding the former aspect, which is the topic of interest in this article, it can be anticipated that VSC-connected

AC systems with high demand and/or with non-controllable renewable plants would be the most benefitted networks from the BESS allocation. However, the placement of these storage systems should be decided based on quantitative analyses. Preferably, these studies should be supported by an efficient approach that suitably exploits the topological structure and fundamental parameters of the hybrid network, as is the case of the present formulation.

II. MODELING OF AC AND DC TRANSMISSION EQUIPMENT

The modeling of AC/DC transmission equipment is briefly reviewed next. This is the starting point for the development of the proposed approach for BESS siting in hybrid networks. The transmission line equivalent circuit models of Fig. 1 can be used to obtain the power flows of AC and DC systems.
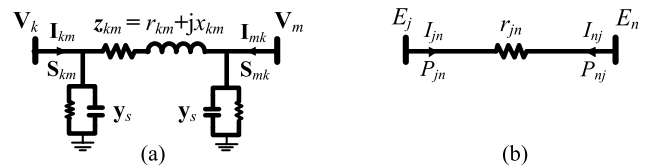

FIGURE 1. Transmission line equivalent models: (a) AC line, (b) DC line.

A. AC POWER FLOWS

Following Fig. 1(a), the current-to-voltage relationship $\mathbf{I} = \mathbf{Y} \times \mathbf{V}$, along with the complex power $\mathbf{S} = \mathbf{V} \times \mathbf{I}^* = \mathbf{V} \times (\mathbf{Y} \times \mathbf{V})^*$, is the starting point for the power flow calculation in AC branches. This is explicitly shown in (1) in terms of meaningful variables. If nodal voltages are expressed in polar form, $\mathbf{V}_k = V_k\, e^{j\theta k}$ and $\mathbf{V}_m = V_m\, e^{j\theta m}$, the active power flow leaving node k towards node m, $P_{km} = \mathrm{Re}\{\mathbf{S}_{km}\}$, is given by (2a). For high-voltage AC systems, the lossless power flow expression shown in (2b) can be obtained by considering that the nodal voltages are close to nominal values and that the angular aperture between adjacent nodes is small, i.e., $g_{kk} = g_{km} \approx 0$, $V_k \approx V_m \approx 1$ pu and $\sin(\theta_k - \theta_m) \approx \theta_k - \theta_m$, respectively.

$$\begin{pmatrix} \mathbf{S}_{km} \\ \mathbf{S}_{mk} \end{pmatrix} = \begin{pmatrix} \mathbf{V}_k & 0 \\ 0 & \mathbf{V}_m \end{pmatrix} \left(\begin{bmatrix} \mathbf{y}_{km} + \mathbf{y}_s & -\mathbf{y}_{km} \\ -\mathbf{y}_{km} & \mathbf{y}_{km} + \mathbf{y}_s \end{bmatrix} \begin{bmatrix} \mathbf{V}_k \\ \mathbf{V}_m \end{bmatrix} \right)^* \tag{1}$$

$$(a)\ \ P_{km} = g_{kk} V_k^2 - V_k V_m \left[g_{km} \cos(\theta_k - \theta_m) \right.$$
$$\left. + b_{km} \sin(\theta_k - \theta_m) \right]$$
$$(b)\ \ P_{km} \approx x_{km}^{-1} V_k V_m \sin(\theta_k - \theta_m) \approx (\theta_k - \theta_m)\, x_{km}^{-1} \tag{2}$$

where the series and shunt admittances are $\mathbf{y}_{km} = (r_{km} + jx_{km})^{-1} = g_{km} + jb_{km}$, $\mathbf{y}_s = g_s + jb_s$, whereas $g_{kk} = g_{km} + g_s$. The power flow in the opposite direction, P_{mk}, can be obtained by exchanging subscripts k and m in (2).

B. DC POWER FLOWS

Similalrly, the nodal current-to-voltage relationship $\mathbf{I} = \mathbf{G} \times \mathbf{E}$ can be used to calculate the DC power flows at nodes k and
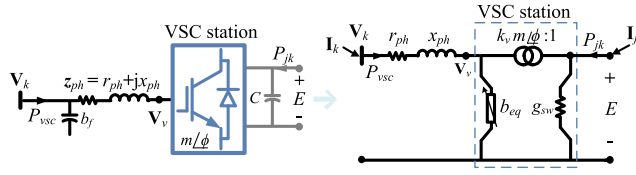
FIGURE 2. Equivalent two-port VSC model for steady-state studies.

FIGURE 3. Four-terminal VSC-based AC/DC power network.

m by using $\mathbf{P} = \mathbf{E} \times \mathbf{I} = \mathbf{E} \times (\mathbf{G} \times \mathbf{E})$. This calculation is shown in (3) for the DC transmission line that connects nodes j and n, see Fig. 1(b). In turn, the power flow P_{jn} leaving node j towards node n is calculated by (4a). It can also be shown that (4b) allows to obtain the power flow for a lossless DC line. This means that the power and current are numerically equal, $P_{jn} \approx I_{jn}$, this being a relationship that holds true when the DC voltages are closer to nominal ones, i.e., $E_j \approx E_n \approx E_{nom}$.

$$\begin{pmatrix} P_{jn} \\ P_{nj} \end{pmatrix} = \begin{pmatrix} E_j & 0 \\ 0 & E_n \end{pmatrix} \left(\begin{bmatrix} g_{jn} & -g_{jn} \\ -g_{jn} & g_{jn} \end{bmatrix} \begin{bmatrix} E_j \\ E_n \end{bmatrix} \right) \quad (3)$$

$$(a) \ P_{jn} = g_{jn} E_j^2 - g_{jn} E_j E_n, \quad (b) \ P_{jn} \approx (E_j - E_n) g_{jn} \quad (4)$$

with $g_{jn} = r_{jn}^{-1}$. The DC power flow in the opposite direction, P_{nj}, is obtained by exchanging subscripts j and n in (4).

C. VSC POWER FLOWS

Fig. 2 shows a typical representation of VSC stations using a two-port model for steady-state studies [1]. It uses the AC-to-DC voltage relationship $\mathbf{V}_v = k_v E m \underline{\phi}$ that describes these three-phase converters, with $k_v = \sqrt{(3/8)}$. The matrix equation resulting from a basic circuit analysis for this VSC model, $\mathbf{I}_{VSC} = \mathbf{Y}_{VSC} \times \mathbf{V}_{VSC}$, is given by (5) using meaningful parameters and variables.

$$\begin{pmatrix} \mathbf{I}_k \\ \mathbf{I}_j \end{pmatrix}$$
$$= \begin{pmatrix} \mathbf{z}_{ph}^{-1} + jb_f & -\mathbf{z}_{ph}^{-1} \times k_v m \angle \phi \\ -\mathbf{z}_{ph}^{-1} \times k_v m \angle -\phi & k_v^2 m^2 \left(\mathbf{z}_{ph}^{-1} + jb_{eq} \right) + g_s \end{pmatrix} \begin{pmatrix} \mathbf{V}_k \\ E \end{pmatrix}$$
$$(5)$$

where $\mathbf{z}_{ph} = r_{ph} + jx_{ph}$ is the coupling impedance, b_f is the filter susceptance, E is the DC voltage, $m \underline{\phi}$ are the modulating variables, b_{eq} is a variable susceptance related to the reactive power exchange with the AC grid, g_{sw} is a shunt conductance that accounts for the converter switching losses [1].

Combining (5) with the power $\mathbf{S}_{VSC} = \mathbf{V}_{VSC} \times (\mathbf{I}_{VSC})^*$, the real power flow P_{vsc} (6a) at the converter AC terminal is obtained after carrying out some complex algebra, using $\mathbf{V}_k = V_k e^{j\theta_k}$ and recalling that $\mathbf{V}_v = k_v E m e^{j\phi}$. Using the same suppositions to obtain (2b), the linear power flow (6b) is obtained for VSC.

$$(a) \quad P_{vsc} = V_k^2 g_{ph}$$
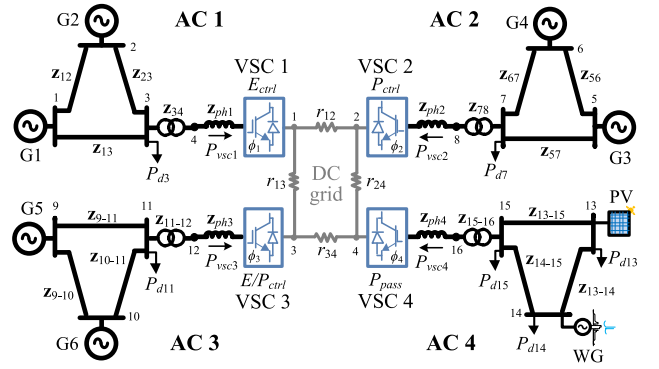$$- V_k V_v \left[g_{ph} \cos(\theta_k - \phi) + b_{ph} \sin(\theta_k - \phi) \right]$$

TABLE 1. VSC control strategies, variables and constraints.

VSC control strategy	Controlled variable	Reference values	Constraint equation
Grid-following, E_{ctrl}	E	E^{ref}	None
Fixed power, P_{ctrl}	P_{vsc}	$P_{vsc} = P^{ref}$	$P^{ref} = (\theta_k - \phi)/x_{ph}$
Grid-forming, E/P_{ctrl}	E, P_{vsc}	E^{ref}, P^{ref}	$P_{vsc} = P^{ref} + K_{ep}(E^{ref} - E)$
Passive, P_{pass}	P_{vsc}	$\cdot \ \phi = \phi^{ref}$	$P_{vsc} = (\theta_k - \phi^{ref})/x_{ph}$

$$(b) \quad P_{vsc} \approx x_{ph}^{-1} V_k V_v \sin(\theta_k - \phi) \approx (\theta_k - \phi) x_{ph}^{-1} \quad (6)$$

where $V_v = k_v E m \approx 1$ pu and $\mathbf{y}_{ph} = (\mathbf{z}_{ph})^{-1} = g_{ph} + jb_{ph}$.

III. MODELING OF VSC-BASED AC/DC NETWORKS BASED ON NODAL POWER INJECTIONS

By way of example, Fig. 3 shows the generic diagram of a VSC-based AC/DC network used to derive the sensitivities-based power loss model. This is a hybrid system that contains four AC systems (AC 1 – AC 4) interfaced with a DC grid through four VSC units (VSC 1 – VSC 4). Note that each converter connects to its AC pairing system by a transformer.

Table 1 summarizes the classical VSC control strategies used in multi-terminal arrangements, indicating the associated control variables, reference values, and constraint equations. It should be recalled that the power flow P_{vsc} of the VSC is given by (6b) regardless of the selected converter strategy. Grid-following and grid-forming control strategies are the preferred choice in recent VSC applications due to their flexible operating features. These deal with voltage control E_{ctrl} in the DC grid and voltage/power droop control E/P_{ctrl}, respectively. With the former, the power can bidirectionally flow in the VSC, between AC and DC grids, to perform voltage control, i.e., there is no power flow constraint associated. Whereas with the latter strategy, it is possible to achieve the so-called power sharing according to the droop control gain K_{ep}. Conversely, the fixed power strategy is the most classical control strategy of all with which the VSC controls its power flow to a constant setpoint value P^{ref}. Both fixed-power and grid-forming strategies are equivalent in steady state since $E = E^{ref}$ and $P_{vsc} = P^{ref}$. For a VSC with passive control strategy, the converter connects

an AC grid either with load only or with non-controllable renewable sources, such as wind (WG) or PV plants. Therefore, the phase-shifting angle of the VSC becomes the angular reference for the AC grid, that is, $\phi = \phi^{ref}$ [1].

Based on the above, the modeling of VSC-based AC/DC networks can be achieved using nodal power injections, i.e., $P_k = P_{gk} - P_{dk} = \Sigma P_{km}$, where P_{km} takes the form of (2b) for the AC subnetworks, (4b) for the DC grid and (6b) for the VSC stations. Following Fig. 3, the power injections associated with AC 1 are shown in (7) in matrix form,

$$\mathbf{P}_{ac1} = \mathbf{B}_{ac1} \, \boldsymbol{\Psi}_{ac1} \qquad (7)$$

with

$$\mathbf{P}_{ac1} = \begin{pmatrix} P_1 \\ \vdots \\ P_4 \end{pmatrix}, \; \mathbf{B}_{ac1} = \begin{pmatrix} B_{11} & \cdots & B_{14} & 0 \\ \vdots & \ddots & \vdots & \vdots \\ B_{41} & \cdots & B_{44} & -x_{ph1}^{-1} \end{pmatrix},$$

$$\boldsymbol{\Psi}_{ac1} = \begin{pmatrix} \theta_1 \\ \vdots \\ \theta_4 \\ \phi_1 \end{pmatrix},$$

where the susceptances are given by $B_{kk} = \Sigma x_{km}^{-1}$, $B_{km} = -x_{km}^{-1}$.

Note that VSC 1 is a grid-following converter E_{ctrl} having no associated power flow constraint, see Table 1. Therefore, there is no need for an additional equation to be added into (7). In contrast, AC 2 is coupled to VSC 2, which features a fixed-power control strategy P_{ctrl}, so the resulting nodal power injection model would be given by,

$$\mathbf{P}_{ac2} = \mathbf{B}_{ac2} \, \boldsymbol{\Psi}_{ac2} \qquad (8)$$

with

$$\mathbf{P}_{ac2} = \begin{pmatrix} P_5 \\ \vdots \\ P_8 \\ P^{ref} \end{pmatrix}, \; \mathbf{B}_{ac2} = \begin{pmatrix} B_{55} & \cdots & B_{58} & 0 \\ \vdots & \ddots & \vdots & \vdots \\ B_{85} & \cdots & B_{88} & -x_{ph2}^{-1} \\ 0 & \cdots & x_{ph2}^{-1} & -x_{ph2}^{-1} \end{pmatrix},$$

$$\boldsymbol{\Psi}_{ac2} = \begin{pmatrix} \theta_5 \\ \vdots \\ \theta_8 \\ \phi_2 \end{pmatrix},$$

where the constraint equation $P^{ref} = (\theta_k - \phi)/x_{ph}$ is included in (8). Following a similar process, the power injection models of AC 3 and AC 4 coupled to VSC 3 and VSC 4 can be obtained, i.e., $\mathbf{P}_{ac3} = \mathbf{B}_{ac3}\boldsymbol{\Psi}_{ac3}$, $\mathbf{P}_{ac4} = \mathbf{B}_{ac4}\boldsymbol{\Psi}_{ac4}$. Additional details about the obtaining of these power flow models for AC/DC grids can be consulted at [22]. On the contrary, the link between AC subsystems and DC grid is provided by the power converters. Taking for instance the case of AC 1 and VSC 1, the power flow equation of VSC 1 (6b) should be equal to that transferred into the DC transmission lines (4b), i.e., $P_{dc1} = P_{g1} - P_{d1} = -P_{vsc1} + P_{12} + \cdots + P_{14}$. This nodal

power balance equation can be expressed by meaningful variables as follows,

$$P_{dc1} = \begin{bmatrix} -x_{ph1}^{-1} & x_{ph1}^{-1} \end{bmatrix} \begin{pmatrix} \theta_4 \\ \phi_1 \end{pmatrix} + \begin{bmatrix} G_{11} & \cdots & G_{14} \end{bmatrix} \begin{pmatrix} E_1 \\ \vdots \\ E_4 \end{pmatrix} \qquad (9)$$

where the conductances are given by $G_{jj} = \Sigma r_{jn}^{-1}, G_{jn} = -r_{jn}^{-1}$.

Note that the voltage phase angle θ_4 and phase-shifting angle ϕ_1 related to VSC 1, also appear in vector $\boldsymbol{\Psi}_{ac1}$ (7). Therefore, applying the same procedure to the rest of converters, VSC 2 – VSC 4, the DC grid power equations would be given by,

$$\mathbf{P}_{dc} = \mathbf{b}_{ph}\boldsymbol{\Phi} + \mathbf{G}_{dc}\mathbf{E}_{dc} \qquad (10)$$

with

$$\mathbf{P}_{dc} = \begin{pmatrix} P_{dc1} \\ \vdots \\ P_{dc4} \end{pmatrix}, \; \mathbf{G}_{dc} = \begin{pmatrix} G_{11} & \cdots & G_{14} \\ \vdots & \ddots & \vdots \\ G_{41} & \cdots & G_{44} \end{pmatrix},$$

$$\mathbf{E}_{dc} = \begin{pmatrix} E_1 \\ \vdots \\ E_4 \end{pmatrix}, \; \mathbf{b}_{ph} = \begin{pmatrix} \mathbf{b}_{ph1} & & \\ & \ddots & \\ & & \mathbf{b}_{ph4} \end{pmatrix}, \; \boldsymbol{\Phi} = \begin{pmatrix} \boldsymbol{\Phi}_{ph1} \\ \vdots \\ \boldsymbol{\Phi}_{ph4} \end{pmatrix},$$

$$\mathbf{b}_{ph\alpha} = \begin{pmatrix} -x_{ph\alpha}^{-1} \\ x_{ph\alpha}^{-1} \end{pmatrix}^T, \; \boldsymbol{\Phi}_{ph\alpha} = \begin{pmatrix} \theta_k \\ \phi_\alpha \end{pmatrix},$$

$$\forall k = \{4, 8, 12, 16\} \quad \text{and} \; \forall \alpha = \{1, 2, 3, 4\}.$$

The representation of AC/DC grids formed by α VSC-coupled AC subnetworks is obtained by suitably combining the models of AC 1 to AC 4, $\mathbf{P}_{ac\alpha} = \mathbf{B}_{ac\alpha}\boldsymbol{\Psi}_{ac\alpha}\forall\alpha = \{1, 2, 3, 4\}$, with that of the DC grid (10). The unified formulation based on nodal power injections is given by (11a), as follows,

$$\begin{pmatrix} \mathbf{P}_{ac1} \\ \vdots \\ \mathbf{P}_{ac\alpha} \\ \mathbf{P}_{dc} \end{pmatrix} = \begin{pmatrix} \mathbf{B}_{ac1} & & \mathbf{0} & \mathbf{0} \\ & \ddots & & \vdots \\ \mathbf{0} & & \mathbf{B}_{ac\alpha} & \mathbf{0} \\ \mathbf{b}'_{ph1} & \cdots & \mathbf{b}'_{ph\alpha} & \mathbf{G}_{dc} \end{pmatrix} \begin{pmatrix} \boldsymbol{\Psi}_{ac1} \\ \vdots \\ \boldsymbol{\Psi}_{ac\alpha} \\ \mathbf{E}_{dc} \end{pmatrix}$$

$$\Rightarrow \quad \begin{array}{l} (a) \; \mathbf{P}_{acdc} = \mathbf{M}_{acdc}\Theta_{acdc} \\ (b) \; \mathbf{P}'_{acdc} = \mathbf{M}'_{acdc}\Theta'_{acdc} \end{array} \qquad (11)$$

where entries $\mathbf{0}$ are zero-padded matrices of suitable orders, $\mathbf{b}'_{ph\alpha}$ are matrices that contain the vectors $\mathbf{b}_{ph\alpha} = [-x_{ph\alpha}^{-1} \; x_{ph\alpha}^{-1}]$ in suitable positions corresponding to the phase angles of the converters' AC terminal θ_k and phase-shifting angle ϕ_α, as observed from (9) for the case of VSC 1.

The solution of (11a) must be preceded by assumptions adopted in the classical power flow theory. That is, (i) for AC grids with controllable generation, the nodal phase angles related to slack generators are set to $\theta_s = 0$; (ii) the DC voltages of grid-following and grid-forming VSC are known a priori $E = E^{ref}$; (iii) for VSC coupled to passive grids with no generation of their own, the phase-shifting angles become the angular reference, $\phi = \phi^{ref} = 0$. The above imply the

removal of rows and columns in (11a) related to the variables cited in (i)-(iii), which leads to the model (11b). Matrix $\mathbf{M}'_{acdc}$ is used to obtain the Injection Shift Factors (ISF) in Section V, which are key elements of the present method.

IV. SENSITIVITIES-BASED AC/DC LOSS MODEL

A. AC/DC TRANSMISSION POWER LOSSES

The operation of BESS can impose changes in the power flows and power losses of the transmission lines that neighbor its connection. Depending on the multiterminal HVDC arrangement and VSC control strategies (see Table 1), power changes could be observed at any of the AC systems or at DC grid. Hence, it is important to quantify the changes in power losses of the transmission equipment that forms the hybrid network. Power losses in series-connected AC branches, such as transmission lines and power transformers, can be estimated by the summation of the powers flowing in both directions, $P_{km} + P_{mk}$, using (2a). The same is also true for the DC lines (4a) and the VSC units (6a). These calculations are shown in (12) for the AC branches P_{ac}^{loss}, VSC stations P_{vsc}^{loss}, and DC lines P_{dc}^{loss}, respectively.

$$
\begin{aligned}
(a) \quad & P_{ac}^{loss} = g_{km} \left(V_k^2 + V_m^2 \right) - 2g_{km} V_k V_m \cos (\theta_k - \theta_m) \\
(b) \quad & P_{vsc}^{loss} = g_{ph} \left(V_k^2 + V_v^2 \right) - 2g_{ph} V_k V_v \cos (\theta_k - \phi) \\
(c) \quad & P_{dc}^{loss} = g_{jn} \left(E_j^2 + E_n^2 \right) - 2g_{jn} E_j E_n
\end{aligned} \tag{12}
$$

where it is assumed that $g_s \approx 0$ in (12a), thus $g_{kk} \approx g_{km}$. With these expressions, a generalized power loss sensitivity model can be developed for VSC-based AC/DC power networks.

B. SENSITIVITIES-BASED POWER LOSSES

For the AC/DC power loss model to be consistent with the proposed method, it is required to derive a linear sensitivities-based power loss model of the AC/DC network. Specifically, it is sought to obtain power loss sensitivities with respect to incremental changes of the AC/DC system state variables. That is to say, $\Delta P_{ac}^{loss}/\Delta \chi_{ac} \; \forall \chi_{ac} : \{V_k, V_m, \theta_k, \theta_m\}$ for the series branches in the AC systems, $\Delta P_{vsc}^{loss}/\Delta \chi_{vsc} \; \forall \chi_{vsc} : \{V_k, V_v, \theta_k, \phi\}$ for the VSC stations, and $\Delta P_{dc}^{loss}/\Delta \chi_{dc} \; \forall \chi_{dc} : \{E_k, E_m\}$ for the DC transmission lines. These are shown in (14), (16), (18), which are obtained by substituting the corresponding partial derivatives of (12a), (12b), (12c) into (13), (15), (17), respectively.

For AC systems:

$$
\begin{aligned}
\Delta P_{ac}^{loss} = {} & \frac{\partial P_{ac}^{loss}}{\partial V_k} \Delta V_k + \frac{\partial P_{ac}^{loss}}{\partial V_m} \Delta V_m + \frac{\partial P_{ac}^{loss}}{\partial \theta_k} \Delta \theta_k \\
& + \frac{\partial P_{ac}^{loss}}{\partial \theta_m} \Delta \theta_m
\end{aligned} \tag{13}
$$

$$
\begin{aligned}
\Delta P_{ac}^{loss} \approx {} & 2g_{km} (V_k - V_m) \begin{bmatrix} 1 & -1 \end{bmatrix} \begin{pmatrix} \Delta V_k \\ \Delta V_m \end{pmatrix} \\
& + 2g_{km} V_k V_m \sin (\theta_k - \theta_m) \begin{bmatrix} 1 & -1 \end{bmatrix} \begin{pmatrix} \Delta \theta_k \\ \Delta \theta_m \end{pmatrix}
\end{aligned} \tag{14}
$$

For VSC stations:

$$
\begin{aligned}
\Delta P_{vsc}^{loss} = {} & \frac{\partial P_{vsc}^{loss}}{\partial V_k} \Delta V_k + \frac{\partial P_{vsc}^{loss}}{\partial V_v} \Delta V_v + \frac{\partial P_{vsc}^{loss}}{\partial \theta_k} \Delta \theta_k \\
& + \frac{\partial P_{vsc}^{loss}}{\partial \phi} \Delta \phi
\end{aligned} \tag{15}
$$

$$
\begin{aligned}
\Delta P_{vsc}^{loss} \approx {} & 2g_{ph} (V_k - V_v) \begin{bmatrix} 1 & -1 \end{bmatrix} \begin{pmatrix} \Delta V_k \\ \Delta V_v \end{pmatrix} \\
& + 2g_{ph} V_k V_v \sin (\theta_k - \phi) \begin{bmatrix} 1 & -1 \end{bmatrix} \begin{pmatrix} \Delta \theta_k \\ \Delta \phi \end{pmatrix}
\end{aligned} \tag{16}
$$

For the DC grid:

$$
\Delta P_{dc}^{loss} = \frac{\partial P_{dc}^{loss}}{\partial E_j} \Delta E_j + \frac{\partial P_{dc}^{loss}}{\partial E_n} \Delta E_n \tag{17}
$$

$$
\Delta P_{dc}^{loss} = 2g_{jn} (E_j - E_n) \begin{bmatrix} 1 & -1 \end{bmatrix} \begin{pmatrix} \Delta E_j \\ \Delta E_n \end{pmatrix} \tag{18}
$$

These terms allow us to obtain power loss sensitivities with respect to significant variables of AC branches $\Delta P_{ac}^{loss}/\Delta \chi_{ac}$ (14), VSC stations $\Delta P_{vsc}^{loss}/\Delta \chi_{vsc}$ (16) and DC lines $\Delta P_{dc}^{loss}/\Delta \chi_{dc}$ (18). These can be further simplified without compromising the essential behavior of power loss variations in the AC/DC system. In high-voltage AC systems, we often assume that voltage variations cause negligible changes in power losses. This idea can also be extended for the AC terminal of VSC units, thus $\Delta V_k \approx \Delta V_m \approx \Delta V_v = 0$ in (14) and (16). Also, it is true that $x_{km} P_{km} = V_k V_m \sin (\theta_k - \theta_m)$ for AC lines (2b), and $x_{ph} P_{kj} = V_k V_v \sin (\theta_k - \phi)$ for VSC stations (6b), remembering that $P_{jn} = g_{jn}(E_j - E_n)$ of (4b). Substituting these relations into (14), (16), (18), we obtain the following,

$$
\Delta P_{ac}^{loss} \approx 2g_{km} x_{km} P_{km} \begin{bmatrix} 1 & -1 \end{bmatrix} \begin{pmatrix} \Delta \theta_k \\ \Delta \theta_m \end{pmatrix} \tag{19}
$$

$$
\Delta P_{vsc}^{loss} \approx 2g_{ph} x_{ph} P_{vsc} \begin{bmatrix} 1 & -1 \end{bmatrix} \begin{pmatrix} \Delta \theta_k \\ \Delta \phi \end{pmatrix} \tag{20}
$$

$$
\Delta P_{dc}^{loss} = 2P_{jn} \begin{bmatrix} 1 & -1 \end{bmatrix} \begin{pmatrix} \Delta E_j \\ \Delta E_n \end{pmatrix} \tag{21}
$$

where these sensitivities are expressed in terms of the most important variables that affect the power loss behavior in AC/DC grids, that is, $\chi_{ac} : \{\theta_k, \theta_m\}$, $\chi_{vsc} : \{\theta_k, \phi\}$, $\chi_{dc} : \{E_j, E_n\}$.

C. GENERALIZATION OF THE SENSITIVITIES-BASED LOSS MODEL

1) AC SUBNETWORKS

In connection with Fig. 3, the power loss sensitivity model for AC 1 and VSC 1 is obtained by applying (19)-(20) to each k-m transmission branch and converter phase reactor of the electrical system. For modeling convenience, power loss sensitivities of AC transmission branches ΔP_{ac}^{loss} and VSC stations ΔP_{vsc}^{loss} can be matrix arranged as follows,

$$
\Delta \mathbf{P}_{ac1}^{loss} = 2\mathbf{g}_{km1} \mathbf{x}_{km1} \mathbf{P}_{km1} \mathbf{A}_{ac1} \Delta \mathbf{\Psi}_{ac1} \tag{22}
$$

with

$$\Delta\mathbf{P}^{loss}_{ac1} = \begin{bmatrix} \Delta P^{loss}_{12} & \cdots & \Delta P^{loss}_{34} & \Delta P^{loss}_{vsc1} \end{bmatrix}^T,$$

$$\mathbf{g}_{km1} = \begin{pmatrix} g_{12} & & \\ & \ddots & \\ & & g_{ph1} \end{pmatrix},$$

$$\mathbf{x}_{km1} = \begin{pmatrix} x_{12} & & \\ & \ddots & \\ & & x_{ph1} \end{pmatrix},$$

$$\mathbf{P}_{km1} = \begin{pmatrix} P_{12} & & \\ & \ddots & \\ & & P_{vsc1} \end{pmatrix},$$

$$\Delta\mathbf{\Psi}_{ac1} = \begin{bmatrix} \Delta\theta_1 & \cdots & \Delta\theta_4 & \Delta\phi_1 \end{bmatrix}^T$$

where $\mathbf{g}_{km}$, $\mathbf{x}_{km}$, $\mathbf{P}_{km}$, are l_{ac}-by-l_{ac} diagonal matrices, with l_{ac} being the number of AC transmission branches including that of the VSC phase reactor. $\mathbf{A}_{ac1}$ is a l_{ac}-by-n_{ac} matrix that denotes the element-node incidence matrix of VSC-coupled AC 1, with n_{ac} being the number of nodes plus one. The n_{ac}-by-1 vector $\Delta\mathbf{\Psi}_{ac1}$ accommodates the changes of AC system phase angles, including that of the VSC phase-shifting angle. $\Delta\mathbf{P}^{loss}_{ac1}$ is a l_{ac}-by-1 vector with the power loss sensitivities of the transmission branches resulting from the electrical coupling between AC 1 and VSC 1. Clearly, a similar model can be obtained for the rest of VSC-connected power systems pertaining to the multi-terminal arrangement, i.e., AC 2 - AC 4. Therefore, equation (22) can be straightforwardly extended to (23) for AC/DC power grids involving α AC subnetworks.

$$\Delta\mathbf{P}^{loss}_{ac} = 2\mathbf{g}_{km}\mathbf{x}_{km}\mathbf{P}_{km}\mathbf{A}_{ac}\,\Delta\mathbf{\Psi}_{ac} \qquad (23)$$

with

$$\Delta\mathbf{P}^{loss}_{ac} = \begin{bmatrix} \Delta\mathbf{P}^{loss}_{ac1} \\ \vdots \\ \Delta\mathbf{P}^{loss}_{ac\alpha} \end{bmatrix}, \quad \Delta\mathbf{\Psi}_{ac} = \begin{bmatrix} \Delta\mathbf{\Psi}_{ac1} \\ \vdots \\ \Delta\mathbf{\Psi}_{ac\alpha} \end{bmatrix},$$

$$\mathbf{g}_{km} = \begin{pmatrix} \mathbf{g}_{km1} & & \\ & \ddots & \\ & & \mathbf{g}_{km\alpha} \end{pmatrix},$$

$$\mathbf{x}_{km} = \begin{pmatrix} \mathbf{x}_{km1} & & \\ & \ddots & \\ & & \mathbf{x}_{km\alpha} \end{pmatrix},$$

$$\mathbf{P}_{km} = \begin{pmatrix} \mathbf{P}_{km1} & & \\ & \ddots & \\ & & \mathbf{P}_{km\alpha} \end{pmatrix},$$

$$\mathbf{A}_{ac} = \begin{pmatrix} \mathbf{A}_{ac1} & & \\ & \ddots & \\ & & \mathbf{A}_{ac\alpha} \end{pmatrix}$$

where $\mathbf{g}_{km}$, $\mathbf{x}_{km}$, $\mathbf{P}_{km}$, $\mathbf{A}_{ac}$, are diagonal matrices of matrices consistent with the α AC systems. Vector $\Delta\mathbf{P}^{loss}_{ac}$ contains the power loss sensitivities of all transmission branches of the α AC systems, whereas vector $\Delta\mathbf{\Psi}_{ac}$ contains the changes of all nodal phase angles and phase-shifting angles of AC systems and VSC stations of the hybrid network, respectively.

2) DC GRID

Following a similar process to that conducted for AC branches, the sensitivities of the DC grid can be obtained. By cautiously applying (21) to each j-n DC line we obtain,

$$\Delta\mathbf{P}^{loss}_{dc} = 2\mathbf{P}_{jn}\mathbf{A}_{dc}\,\Delta\mathbf{E}_{dc} \qquad (24)$$

with

$$\Delta\mathbf{P}^{loss}_{dc} = \begin{pmatrix} \Delta P^{loss}_{12} \\ \vdots \\ \Delta P^{loss}_{34} \end{pmatrix}, \quad \mathbf{P}_{jn} = \begin{pmatrix} P_{12} & & \\ & \ddots & \\ & & P_{34} \end{pmatrix},$$

$$\Delta\mathbf{E}_{dc} = \begin{pmatrix} \Delta E_1 \\ \vdots \\ \Delta E_4 \end{pmatrix},$$

where $\mathbf{P}_{jn}$ denotes an l_{dc}-by-l_{dc} diagonal matrix containing the DC power flows, with l_{dc} being the number of DC lines. $\mathbf{A}_{dc}$ is an l_{dc}-by-n_{dc} matrix representing the element-node incidence matrix of the DC grid, whose number of nodes is n_{dc}. The n_{dc}-by-1 vector $\Delta\mathbf{E}_{dc}$ contains the changes of DC nodal voltages, whereas the l_{dc}-by-1 vector $\Delta\mathbf{P}^{loss}_{dc}$ contains the power loss sensitivities of the DC transmission lines.

The AC and DC power loss sensitivities (23)-(24) depend on the power flows, $\mathbf{P}_{km}$ and $\mathbf{P}_{jn}$, along with the state variables contained in $\Delta\mathbf{\Psi}_{ac}$, $\Delta\mathbf{E}_{dc}$ that affect the power loss behavior. Returning to the power flow modeling for AC branches and VSC coupling phase reactors, $P_{km} = (\theta_k - \theta_m)/x_{km}$ and $P_{vsc} = (\theta_k - \phi)/x_{ph}$, the model shown in (25) can be obtained for the power flows of AC 1 (see Fig. 1) by using the alternative equations $x_{km} P_{km} = (\theta_k - \theta_m)$ and $x_{ph} P_{vsc} = (\theta_k - \phi)$.

$$\begin{pmatrix} x_{12}P_{12} \\ x_{13}P_{13} \\ x_{23}P_{23} \\ x_{34}P_{34} \\ x_{ph1}P_{vsc1} \end{pmatrix} = \begin{pmatrix} 1 & -1 & 0 & 0 & 0 \\ 1 & 0 & -1 & 0 & 0 \\ 0 & 1 & -1 & 0 & 0 \\ 0 & 0 & 1 & -1 & 0 \\ 0 & 0 & 0 & 1 & -1 \end{pmatrix} \begin{pmatrix} \theta_1 \\ \theta_2 \\ \theta_3 \\ \theta_4 \\ \phi_1 \end{pmatrix}$$

$$\Rightarrow \quad \mathbf{x}_{km1}\mathbf{P}_{ac1} = \mathbf{A}_{ac1}\,\mathbf{\Psi}_{ac1} \qquad (25)$$

which can be extended for the α VSC-coupled AC systems, in a similar way as it was conducted for (23), that is,

$$\mathbf{x}_{km}\mathbf{P}_{ac} = \mathbf{A}_{ac}\,\mathbf{\Psi}_{ac} \qquad (26)$$

where $\mathbf{P}_{ac} = [\mathbf{P}_{ac1}, \cdots, \mathbf{P}_{ac\alpha}]^T$ is an l_{ac}-by-1 vector with the power flows of the α AC systems, recalling that $\mathbf{x}_{km}$ is an l_{ac}-by-l_{ac} diagonal matrix and $\mathbf{A}_{ac}$ is the element-node incidence matrix. Similarly, the DC grid power flows, $r_{jn} P_{jn} = (E_j - E_n)$, can be related to the state variables as follows,

$$\mathbf{r}_{jn}\mathbf{P}_{dc} = \mathbf{A}_{dc}\,\mathbf{E}_{dc} \qquad (27)$$

where $\mathbf{r}_{jn}$ denotes an l_{dc}-by-l_{dc} diagonal matrix containing the resistances of the DC transmission lines. The incremental

form of (26), $\mathbf{x}_{km}\Delta\mathbf{P}_{ac} = \mathbf{A}_{ac} \Delta\Psi_{ac}$, can be substituted into (23) to obtain (28a), while the incremental form of (27), $\mathbf{r}_{jn}\Delta\mathbf{P}_{dc} = \mathbf{A}_{dc} \Delta\mathbf{E}_{dc}$, can be substituted into (24) to obtain (28b). The AC/DC power loss sensitivities (28) are now expressed as functions of incremental power flow changes $\Delta\mathbf{P}_{ac}$, $\Delta\mathbf{P}_{dc}$, instead of incremental state variable changes $\Delta\Psi_{ac}$, $\Delta\mathbf{E}_{dc}$. In this way, ISF can be directly combined with (28), as shown in the next section. The use of ISF is more adequate for large-scale systems than it is the use of nodal phase angles, particularly when resolving models of greater complexity, as is the case of VSC-based AC/DC power networks.

$$
\begin{aligned}
(a) \quad & \Delta\mathbf{P}_{ac}^{loss} = 2\mathbf{g}_{km}\mathbf{x}_{km}^2\mathbf{P}_{km} \Delta\mathbf{P}_{ac} \\
(b) \quad & \Delta\mathbf{P}_{dc}^{loss} = 2\mathbf{r}_{jn}\mathbf{P}_{jn} \Delta\mathbf{P}_{dc}
\end{aligned} \tag{28}
$$

V. PROPOSED APPROACH FOR THE OPTIMUM BESS ALLOCATION IN AC/DC NETWORKS USING ISF

Power injections by BESS will force some of the AC/DC state variables shown in (11) to change, causing redistributions of power flows and power loss changes. To quantify the impact of BESS on the power flows and losses, Injection Shift Factors (ISF) can be used for VSC-based AC/DC grids, just as in the case of pure AC systems [23]. The ISF originate from a system-wide modeling based on power injections, as described in Section III. Thus, the changes in the system variables due to nodal power changes can be established by (11b), i.e.,

$$
\mathbf{P}'_{acdc} = \mathbf{M}'_{acdc} \Theta'_{acdc} \Rightarrow \Delta\Theta'_{acdc} = \mathbf{F}_{acdc} \Delta\mathbf{P}'_{acdc} \tag{29}
$$

where the terms of $\mathbf{F}_{acdc} = \mathbf{M}'^{-1}_{acdc}$ signify $\Delta\chi_{acdc}/\Delta P_k \forall \chi_{acdc}$: $\{\theta_k, \phi_\alpha, E_k\}$, whereas $\Delta\Theta'_{acdc}$ contains the changes in the state variables and $\Delta\mathbf{P}'_{acdc}$ represents the increments in the nodal power injections. From (29), if there is a power injection change at the i-th bus of the AC/DC network, it follows that,

$$
(a) \quad
\begin{aligned}
\Delta\theta_1 &= F_{1i} \Delta P_i \\
&\vdots \\
\Delta\theta_k &= F_{ki} \Delta P_i \\
&\vdots \\
\Delta\theta_m &= F_{mi} \Delta P_i
\end{aligned}
\quad (b) \quad
\begin{aligned}
\Delta E_1 &= F_{1i} \Delta P_i \\
&\vdots \\
\Delta E_j &= F_{ji} \Delta P_i \\
&\vdots \\
\Delta E_n &= F_{ni} \Delta P_i
\end{aligned}
\tag{30}
$$

where (30a) shows the changes in voltage phase angles $\Delta\theta$ when a nodal power change ΔP_i occurs in i-th bus of the network. Similarly, (30b) shows the changes in the nodal voltages of the DC grid ΔE for a nodal power change in i-th bus of the network. The terms F are taken from $\mathbf{F}_{acdc}$ (29).

Since the ISF denote changes in power flows with respect to power injections [22], [23], therefore (31) holds true.

$$
(a) \quad \Gamma_{km,i} = \frac{\Delta P_{km}}{\Delta P_i}, \quad (b) \quad \Gamma_{jn,i} = \frac{\Delta P_{jn}}{\Delta P_i} \tag{31}
$$

where $\Gamma_{km,i}$ are ISF for AC branches connecting nodes k and m, and $\Gamma_{jn,i}$ are ISF for DC lines connecting nodes j and n. Both enable the estimation of the power flow changes,

ΔP_{km} and ΔP_{jn}, with respect to nodal power injections in the AC/DC system ΔP_i. Because the AC and DC power flows can be calculated using P_{km} with (2b) and P_{jn} with (4b), these powers can be combined with (30)-(31) to obtain the ISF as follows,

$$
\begin{aligned}
(a) \quad \Gamma_{km,i} &= \frac{\Delta P_{km}}{\Delta P_i} = \frac{1}{x_{km}}\left(\frac{\Delta\theta_k}{\Delta P_i} - \frac{\Delta\theta_m}{\Delta P_i}\right) \\
&= \frac{1}{x_{km}}\left(F_{ki} - F_{mi}\right) \\
(b) \quad \Gamma_{jn,i} &= \frac{\Delta P_{jn}}{\Delta P_i} = \frac{1}{r_{jn}}\left(\frac{\Delta E_j}{\Delta P_i} - \frac{\Delta E_n}{\Delta P_i}\right) \\
&= \frac{1}{r_{jn}}\left(F_{ji} - F_{ni}\right)
\end{aligned}
\tag{32}
$$

where the ISF for AC branches $\Gamma_{km,i}$ (32a), and those for DC lines $\Gamma_{jn,i}$ (32b), are now explicitly formulated as function of coefficients F of matrix $\mathbf{F}_{acdc}$, AC transmission reactances x_{km} and DC line resistances r_{jn}. Since these ISF permit to calculate the power flow changes with respect to power injections, the relationship $\Delta P_{km} = \Gamma_{km,i} \times \Delta P_i$ holds true for AC branches and $\Delta P_{jn} = \Gamma_{jn,i} \times \Delta P_i$ for DC lines. These can be properly matrix arranged for simplicity of subsequent calculations. That is,

$$
\begin{pmatrix} \Delta P_{km} \\ \vdots \\ \Delta P_{jn} \\ \vdots \end{pmatrix}
=
\begin{pmatrix}
\Gamma_{km,1} & \cdots & \Gamma_{km,i} & \cdots & \Gamma_{km,n} \\
\vdots & \cdots & \vdots & \cdots & \vdots \\
\Gamma_{jn,1} & \cdots & \Gamma_{jn,i} & \cdots & \Gamma_{jn,n} \\
\vdots & \cdots & \vdots & \cdots & \vdots
\end{pmatrix}
\begin{pmatrix} \Delta P_1 \\ \vdots \\ \Delta P_i \\ \vdots \\ \Delta P_n \end{pmatrix}
$$

$$
\Rightarrow \Delta\mathbf{P}_{acdc} = \mathbf{\Gamma}_{acdc} \Delta\mathbf{P}_i \tag{33}
$$

where $\mathbf{\Gamma}_{acdc}$ is an l-by-n matrix with the ISF of the AC/DC grid, with $n = n_{ac} + n_{dc}$ being the total number of nodes and $l = l_{ac} + l_{dc}$ being the total number of lines of the hybrid system. The l-by-1 vector $\Delta\mathbf{P}_{acdc} = [\Delta\mathbf{P}_{ac}, \Delta\mathbf{P}_{dc}]^T$ contains the power flow incremental changes, and the n-by-1 vector $\Delta\mathbf{P}_i$ comprises the incremental changes in nodal power injections, with $i\forall\{1, \cdots, n\}$.

In this work, BESS power injections P_{bess} are governed by a predefined operating strategy and must be placed in vector $\Delta\mathbf{P}_i$ to quantify the power loss changes in the entire AC/DC network. The power output P_{bess} is used as a known input in this formulation. In this kind of application, the storage system is expected to manage high amounts of energy during its operation. Therefore, the power P_{bess} should be established observing critical operating characteristics of the BESS such as thermal limits, charging/discharging ramp rates, power reserve, minimum/maximum storage capacity, among others.

The incremental power flows (33) can be combined with (28) to obtain a unified sensitivities-based loss model,

while redefining $\Delta\mathbf{P}_i \Rightarrow \Delta\mathbf{P}_{bess}$ for clarity of ensuing derivations. This is shown below,

$$\Delta\mathbf{P}^{loss}_{acdc} = \begin{pmatrix} \Delta\mathbf{P}^{loss}_{ac} \\ \Delta\mathbf{P}^{loss}_{dc} \end{pmatrix} = \begin{pmatrix} \mathbf{K}_{ac} & \mathbf{0} \\ \mathbf{0} & \mathbf{K}_{dc} \end{pmatrix} \mathbf{\Gamma}_{acdc}\,\Delta\mathbf{P}_{bess} \quad (34)$$

where $\mathbf{K}_{ac} = 2\mathbf{g}_{km}\times(\mathbf{x}_{km})^2\times\mathbf{P}_{km}$, $\mathbf{K}_{dc} = 2\mathbf{r}_{jn}\times\mathbf{P}_{jn}$. Vector $\Delta\mathbf{P}^{loss}_{acdc}$ contains the incremental losses of AC and DC lines, and $\mathbf{0}$ are zero-padded matrices of suitable orders. The power loss sensitivity model given by (34) is based on both injection shift factors $\mathbf{\Gamma}_{acdc}$ and BESS power $\Delta\mathbf{P}_{bess}$. Considering a set of operation periods for the AC/DC grid, the best candidate node for the BESS allocation can be identified as follows,

$$(a)\ \Delta\mathbf{P}^{loss}_{tot} = \sum_{t=1}^{t_{op}}\Delta\mathbf{P}^{loss}_{acdc(t)}, \quad (b)\ \min\ \Delta\mathbf{P}^{loss}_{tot}\ \Rightarrow\ n_{bess}$$

$$(35)$$

where n_{bess} is the row index related to the minimum value obtained in vector $\Delta\mathbf{P}^{loss}_{tot}$ and t_{op} is the total operating points of the demand and generation patterns, say $\forall t \in \{1,\ldots,t_{op}\}$.

The flow chart of Fig. 4 summarizes the main steps of the new approach. (i) The first step is the input of network parameters with which various terms are built up, e.g., $\mathbf{g}_{km}$, $\mathbf{x}_{km}$, $\mathbf{r}_{jn}$, including the ISF matrix $\mathbf{\Gamma}_{acdc}$. (ii) Secondly, a load flow study based on ISF is conducted to obtain the AC/DC power flows $\mathbf{P}_{km}$, $\mathbf{P}_{jn}$. (iii) Thirdly, with these power flows and the BESS power P_{bess} placed in $\Delta\mathbf{P}_{bess}$, the power loss changes in the network can be obtained for all time periods. Given the modeling nature of the hybrid systems, the present approach permits to effectively identify the optimum BESS connection in fair-sized VSC-based AC/DC networks, as confirmed by the case studies in Section VII.
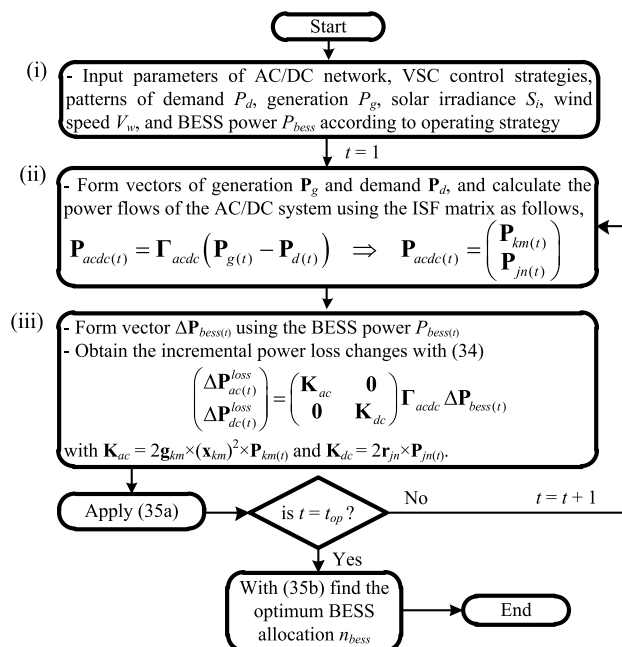

FIGURE 4. Flow chart that summarizes the proposed approach.

VI. RENEWABLE GENERATION MODELS

To place due emphasis on the power loss minimization by BESS allocation in AC/DC networks, simplified but practical renewable generation models are used in this work. The power production by wind generation (WG) and PV plants are regarded to have direct relationships to wind speed and solar irradiance, respectively, as expressed by (36). It follows that both renewable plants can be described by the normalized curves of Fig. 5. Specifically, Fig. 5(a) bears a similarity to the well-known WG power curve, whereas Fig. 5(b) is consistent with the fact that the power output of a PV plant is proportional to solar irradiance.
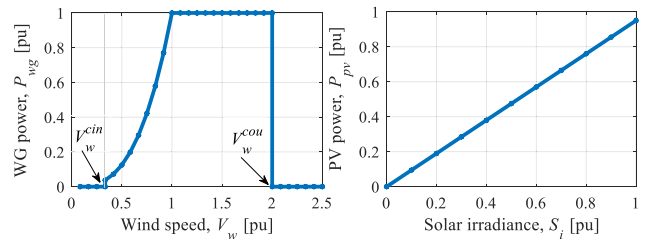

FIGURE 5. Normalized power curves of WG and PV plants.

$$(a)\ P_{wg} = \begin{cases} 0 & V_w^{cin} > V_w > V_w^{cou} \\ P_{wg}^{nom}V_w^3 & V_w^{cin} \le V_w < V_w^{nom} \\ P_{wg}^{nom} & V_w^{nom} \le V_w \le V_w^{cou}, \end{cases}$$

$$(b)\ P_{pv} = P_{pv}^{nom}k_s S_i \quad (36)$$

where P_{wg}, P_{pv} are the power generations of WG and PV plants, with P_{wg}^{nom}, P_{pv}^{nom} being their nominal powers. V_w is the wind speed of the WG with V_w^{cin}, V_w^{nom}, V_w^{cou} denoting the cut-in, nominal, cut-out wind speeds. S_i is the solar irradiance of the PV plant with k_s being the slope of the curve P_{pv} vs. S_i.

The inclusion of renewable sources can affect the final BESS allocation, particularly when there is a massive integration of non-controllable power sources. Considering uncertainty modeling for renewable energy and system load could help reduce possible errors on its siting in the network. This functionality can be investigated in a future work to combine it with the present method.

VII. CASE STUDIES
A. FOUR-TERMINAL AC/DC GRID – VALIDATION TEST

The VSC-based AC/DC network of Fig. 3 is used to validate the present method for the optimum allocation of a 25-MW BESS operating with the so-called energy time shift strategy [24]. This hybrid network contains four AC networks (AC 1 – AC 4) with a total 900-MW nominal load. Systems AC 1 to AC 3 have two synchronous generators each, whereas AC 4 has two non-controllable renewable plants, that is, one 30-MW solar power plant and one 30-MW wind power plant. The multi-terminal HVDC link is formed by four 200-MVA VSC stations (VSC 1 – VSC 4), with each converter featured by a different control strategy according to Table 1. That
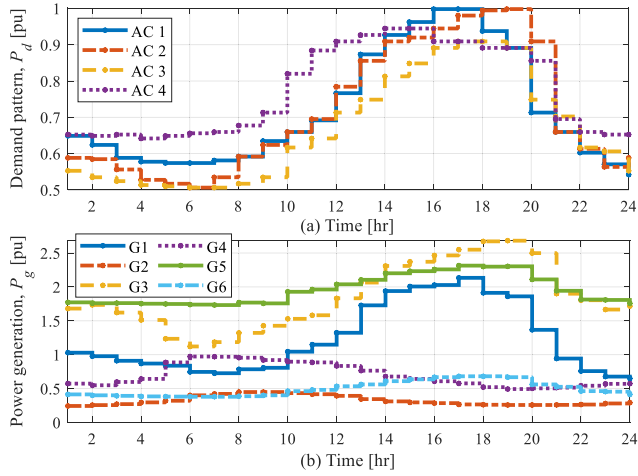
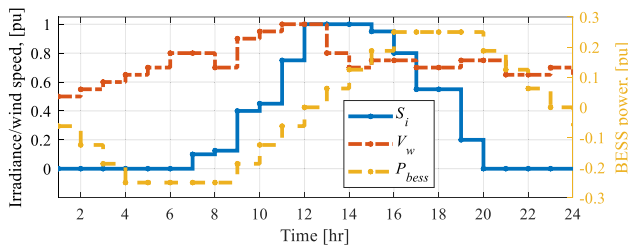**FIGURE 6.** Normalized demand pattern and power generation for an operation day.

FIGURE 7. Solar irradiance S_i, wind speed V_w and BESS power P_{bess}.

FIGURE 8. (a) Hourly incremental losses $\Delta \mathbf{P}_{acdc}^{loss}$ and (b) Total incremental losses $\Delta \mathbf{P}_{tot}^{loss}$ for different connections of the BESS.

FIGURE 9. Power losses obtained by load flow studies with BESS in different system nodes: (a) Hourly losses P_{acdc}^{loss}, (b) Total losses P_{tot}^{loss}.

is, VSC 1 is a grid-following converter E_{ctrl}, with $E^{ref} = 2.0$ p.u.; VSC 2 is a fixed-power converter P_{ctrl}, with $P^{ref} = 1.0$ p.u; VSC 3 is a grid-forming converter E/P_{ctrl}, with $E^{ref} = 2.0$ p.u., $P^{ref} = 1.0$ p.u and $K_{ep} = 50$; and VSC 4 features a passive control strategy P_{pass}, with $\phi^{ref} = 0$. The rest of parameters are given in the Appendix using a 100 MVA base power. Generators G1, G3, G5, which are connected to nodes 1, 5 and 9, respectively, are regarded as slack generators for AC 1 – AC 3, with their nodal phase angles set to $\theta_1 = \theta_5 = \theta_9 = 0$. A typical operation day is considered for this network, $\forall t \in \{1\text{-}24\}$ hr, which is described by the normalized demand patterns P_d and power generations P_g for G1 – G6 given in Fig. 6. Similarly, the forecasted solar irradiance S_i and wind speed V_w of the 30-MW PV and WG power plants are both shown in Fig. 7 in normalized quantities. The charging and discharging operations of the 25-MW BESS to be installed are described by P_{bess} in Fig. 7.

Using these conditions, the hourly incremental power losses $\Delta \mathbf{P}_{acdc}^{loss}$ and total incremental losses $\Delta \mathbf{P}_{tot}^{loss}$ obtained for the AC/DC grid are given in Fig. 8, as calculated in step (iii) of the proposed method. Fig. 8(a) shows that for nodes 1, 5, 9 which are related to slack generators of AC 1 – AC 3, the incremental power losses are $\Delta P_{acdc}^{loss} = 0$, as expected. From 1 hr to 12 hr, the AC/DC network experiences power loss increases $\Delta P_{acdc}^{loss} > 0$ when the BESS connects at most of the nodes. This is so because the BESS operates in charging
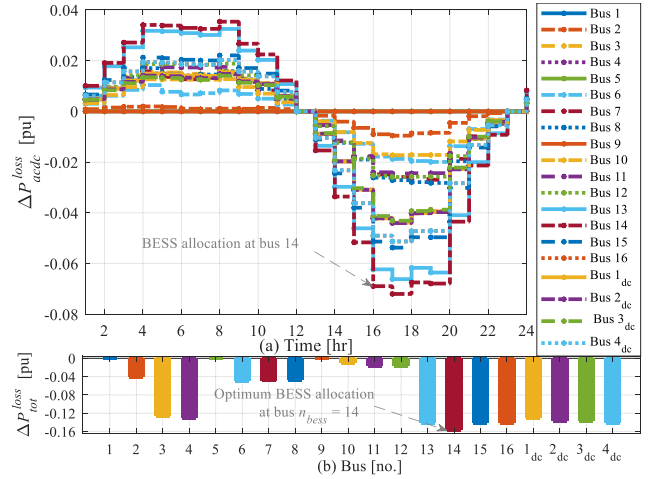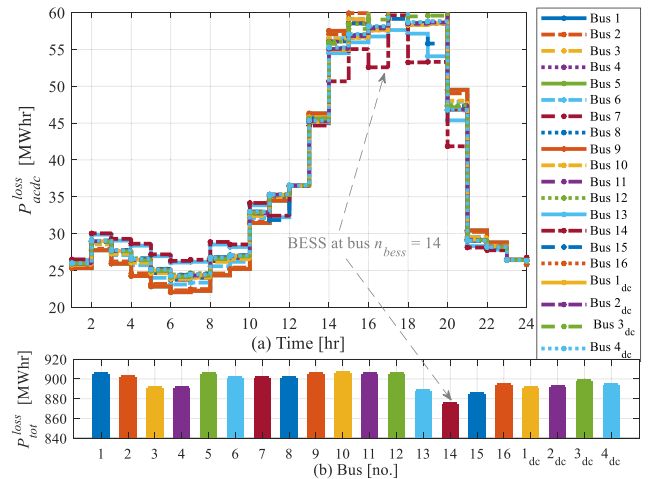
mode $P_{bess} < 0$ consuming power during 1 - 12 hr, see Fig. 7. Subsequently, for period 13 - 24 hr the BESS operates in discharging mode thereby generating power $P_{bess} > 0$, causing transmission losses to be reduced $\Delta P_{acdc}^{loss} < 0$. Note that power loss decreases are observed from 13 hr onwards if the BESS connects at any of the AC/DC system nodes. These facts can be observed more clearly in the total loss increments $\Delta P_{tot}^{loss} \; \forall t \in \{1\text{-}24\}$ hr provided in Fig. 8(b). This figure also shows that the five nodes with the minimum total incremental losses due to BESS power injections are nodes 13 – 16, which take the values $\Delta P_{tot}^{loss} = \{-0.1405, \mathbf{-0.1561}, -0.1419, -0.1406\}$ pu, respectively. This is a reasonable result since these nodes belong to AC 4, which has high demand and no local controllable generation of its own, noting that for 7 hr > t > 20 hr there is no PV generation available. Certainly, the minimum incremental power loss $\min(\Delta P_{tot}^{loss}) = \mathbf{-0.1561}$ pu occurs for bus 14. According to (35b), the best candidate node
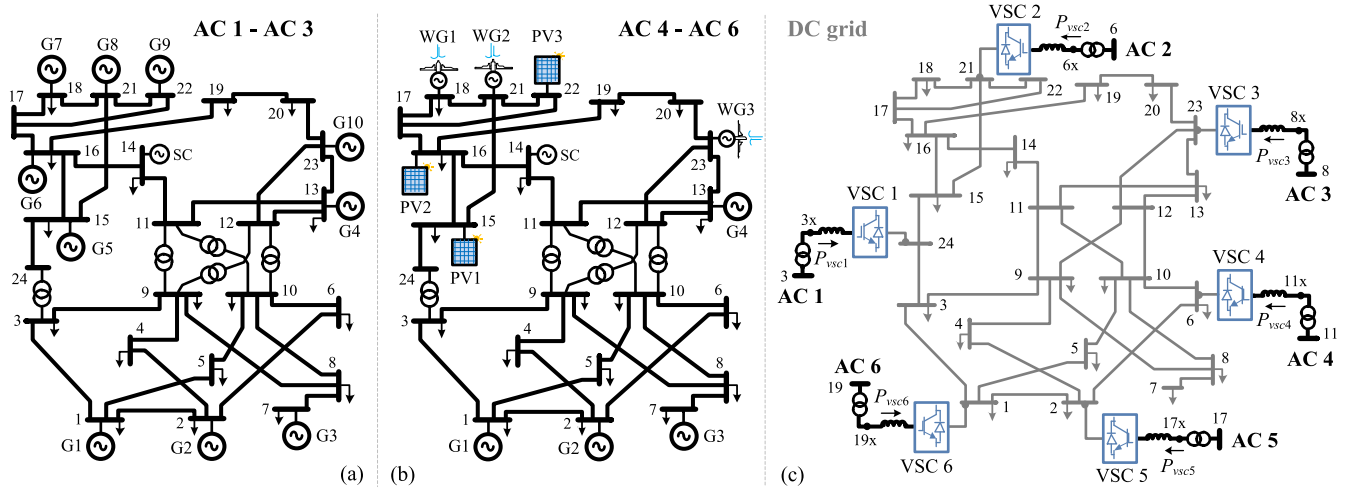
FIGURE 10. (a) IEEE RTS 24-bus test system, (b) with four renewable plants; (c) 24-bus DC grid with six VSC-connected AC networks (AC 1 – AC 6).

for the BESS allocation is $n_{bess} = 14$, which happens to be the node where the largest load and WG plant are placed in AC 4.

1) VALIDATION OF THE PROPOSED APPROACH

One simplified yet effective way to validate the BESS allocation is by running comprehensive power flow studies. Load flow analyses permit to obtain the power losses produced by the BESS connection at any of the AC/DC system nodes (one at a time). With these results, identifying the BESS connection that causes the minimum power losses is a direct task to carry out. To this end, the nonlinear load flow model of the four-terminal VSC-based AC/DC grid should be resolved by using an appropriate load flow method for multi-terminal VSC-HVDC links available in the open literature [1]. However, to obtain suitable results, the same VSC control strategies, demand P_d and generation P_g of Fig. 6, PV generation P_{pv}, WG generation P_{wg} and BESS power P_{bess} of Fig. 7 must be considered in these load flow studies.

According to the above, the hourly power losses P_{acdc}^{loss} calculated by load flow analysis are shown in Fig. 9(a), and the total power losses P_{tot}^{loss} $\forall t \in \{1\text{-}24\}$ hr are given in Fig. 9(b). Note that the minimum network losses are between 20 MWhr to 25 MWhr for low demand conditions $\forall t \in \{4\text{-}8\}$ hr, whereas maximum losses are among $55 \sim 60$ MWhr for peak demand conditions $\forall t \in \{14\text{-}20\}$ hr. For this case study, the power losses observed in Fig. 9(a), represent between 4% - 7% of the generation shown in Fig. 6 and Fig. 7. As mentioned before, the total minimum power losses occur when the BESS is placed at AC 4. This can be corroborated by looking at the results for nodes 13 – 16 given in Fig. 9(b), whose calculated power losses are $P_{tot}^{loss} = \{887.73, \mathbf{874.91}, 884.49, 894.03\}$ MWhr, respectively. Thus, it follows that the minimum power loss is $P_{tot}^{loss} = \mathbf{874.91}$ MWhr for bus 14. It can be concluded anew that the BESS must be installed at bus $n_{bess} = 14$ to guarantee power loss minimization. This validates the present method for BESS allocation in VSC-based AC/DC networks.

TABLE 2. VSC parameters in p.u. and control strategies.

VSC	Control strategy	Reference values	Droop gain	Phase reactor z_{ph} Transformer z_{tr}
1	E_{ctrl}	$E^{ref} = 2.0$	---	
2	E/P_{ctrl}	$P^{ref} = 1.0$	$K_{ep} = 250$	
3	E_{ctrl}	$E^{ref} = 2.0$	---	$z_{ph} = 0.003 + j0.03$
4	E/P_{ctrl}	$P^{ref} = 2.5$	$K_{ep} = 250$	$z_{tr} = 0.001 + j0.03$
5	E/P_{ctrl}	$P^{ref} = 3.0$	$K_{ep} = 250$	
6	P_{ctrl}	$P^{ref} = 4.5$	---	

B. SIX-TERMINAL VSC-BASED AC/DC NETWORK

The six-area electrical system depicted in Fig. 10(a) – (c) is used to exemplify the practicality of the proposed approach. This is a hybrid VSC-based AC/DC power network formed by interconnecting the IEEE RTS 24-bus test system six times [25] through 500-MVA converter stations VSC 1 – VSC 6. Notice that stations VSC 1, 3 are grid-following converters responsible for voltage control, VSC 2, 4, 5 are grid-forming converters featuring voltage/power droop control, whereas VSC 6 is a converter with fixed-power control strategy. Their parameters are reported in Table 2 in per unit for a 100-MW base power. On the other hand, power networks AC 4 – AC 6 have been slightly modified to incorporate renewable plants. Specifically, conventional units G5, G6, G9 are replaced by PV plants PV1 – PV3, respectively, carrying the same nominal power capacities. Likewise, generators G7, G8, G10 are replaced by WG plants WG1 – WG3, respectively, as indicated in Fig. 10(b). It should also be indicated that the G4 generators of AC 1 – AC 6 are set as slack generators for their corresponding power grids. Fig. 10(c) shows that the 24-bus DC grid has the same transmission grid topology as that of the IEEE RTS 24-bus test system, with the parameters recalculated for the new converter base power of 500 MVA, see the Appendix. In sum, this six-area VSC-based AC/DC network contains 60 generating units, 18 renewable power plants, and 174 nodes, including the six internal nodes of VSC stations, that is, those related to
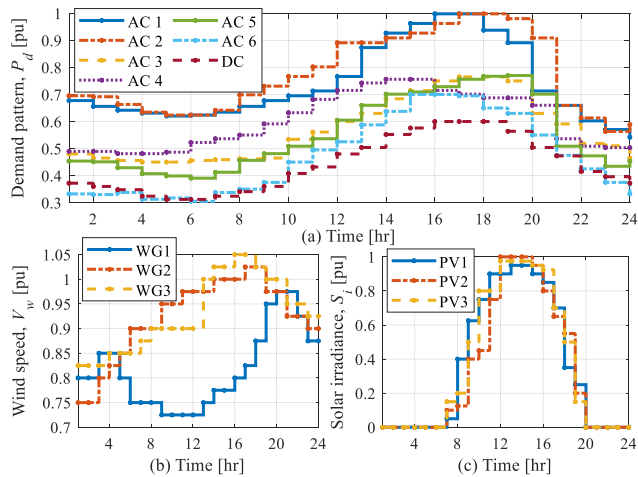
FIGURE 11. Normalized patterns of (a) demand P_d, (b) wind speed V_w, and (c) solar irradiance S_i for a typical operation day.

FIGURE 12. Programmed BESS power injection and selected power flow results: (b) power generated by G4 in AC 1 – AC 6, (c) VSC power flows.

FIGURE 13. Hourly incremental losses ΔP_{acdc}^{loss} for five selected nodes.

the connection point 'x' between coupling impedances $\mathbf{z}_{ph}$ and transformers $\mathbf{z}_{tr}$, see Fig. 10(c). The 24-hour operation horizon of this electrical system is characterized by different conditions of demand P_d for each control area AC1 – AC6 and DC grid, wind speeds V_w for WG1 – WG3, and solar irradiances S_i for PV1 – PV3, all this according to the patterns provided in Fig. 11.

For this case study, it is intended to optimally allocate one 50-MW BESS, whose charge/discharge operations are described by the power injection P_{bess} shown in Fig. 12(a). Using these operating conditions, the approach developed summarized by Fig. 4 is run $\forall t \in \{1\text{-}24\}$ hr. The second step (ii) of the method produces the results provided in Fig. 12(b)-(c), recalling that this is related to steady-state power flow calculations of the AC/DC network by means of ISF. Selected power flow results are reported in these figures. The output powers by the G4 slack generators are given in Fig. 12(b) and the VSC power flows are provided in Fig. 12(c) in per unit for a 100-MW base power. Interesting observations can be made from these results. For example, note that P_{g4} of AC 1 and AC 3 are the ones that follow more closely the hourly demand curves of their corresponding areas, see Fig. 12(b). These behaviors are like those obtained for the VSC power flows P_{vsc} of VSC 1 and VSC 3, see Fig. 12(c). The reason is that since these converters exert DC voltage control E_{ctrl}, their power flows freely through them, with the slack generators of AC 1 and AC 3 compensating for the power changes occurring in the DC grid demand. Furthermore, it is noted from Fig. 12(b) that generators G4 of AC 2, 4, 5 respond according to local demands and renewable power generation in their respective areas. In contrast, power flows of the grid-forming converters VSC 2, 4, 5 slightly vary over time, in accordance with their droop control gains, to assist the DC grid in counteracting the nodal voltage deviations due to demand changes. In sharp contrast, the power flow of VSC 6 remains constant at $P_{vsc6} = 4.5$ pu during the
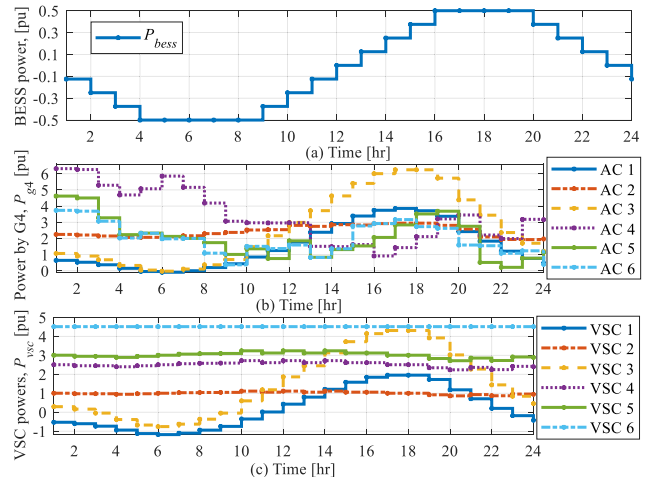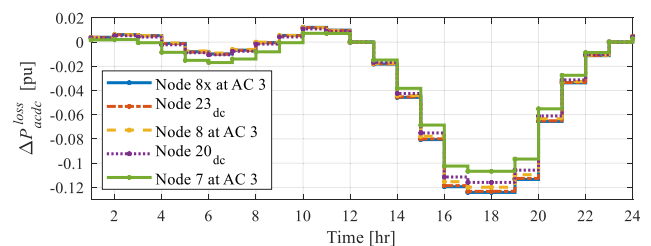
operation horizon due to its fixed-power control strategy P_{ctrl}, as expected.

Of the 174 nodes comprising the AC/DC network, the five nodes with minimum incremental losses ΔP_{acdc}^{loss} are reported in Fig. 13, as obtained by step (iii) of the developed approach, see Fig. 4. Note that most of these nodes neighbor the converter VSC 3. For example, nodes 8x and 8 are related to the AC terminal of this converter which belong to AC 3, whereas node 23_{dc} corresponds to the DC port of VSC 3. In turn, node 20_{dc} of the DC grid is directly linked to node 23_{dc} through a DC transmission line, see Fig. 10(c). This is the result of the severe power flow variations experienced by VSC 3 during the operation horizon, as previously discussed for Fig. 12(c). Table 3 presents the total loss increments $\Delta P_{tot}^{loss} \ \forall t \in \{1\text{-}24\}$ hr for these five nodes from which it can be concluded that the best candidate node for BESS allocation is $n_{bess} = 8x$ at AC 3.

VIII. CONCLUSION

This work introduced advanced modeling features for the power loss minimization by BESS allocation in AC/DC networks. The proposed approach considers multiterminal schemes formed by VSC stations with grid-following, grid-forming, fixed-power control strategies, including converters that interface passive grids with no generation of their own or with non-controlled, intermittent renewable sources. This method is based on incremental modeling of transmission

TABLE 3. Total Loss Increments and BESS allocation n_{bess}.

Node	8x at AC 3	23_{dc} at DC grid	8 at AC 3	20_{dc} at DC grid	7 at AC 3
ΔP_{tot}^{loss}	**-0.7145**	-0.7104	-0.6871	-0.6755	-0.6680
	min(ΔP_{tot}^{loss}) = **-0.7145** pu $\Rightarrow n_{bess}$ = 8x at AC 3				

losses in terms of nodal power injections in AC networks and DC grid. The sensitivities-based power loss model is formulated as function of injection shift factors and BESS power injections governed by a chosen operating strategy. To validate the approach and showcase its practicality, two case studies were conducted in the article. In low demand hours, the hybrid system was shown to face loss increments, with the opposite occurring in peak demand hours, all of this caused by the charge and discharge operations of the BESS, respectively. The nodes most benefitted by the BESS connection are effectively detected by using this new tool. One with which transmission system operators can promptly recognize where BESS must be allocated to make VSC-based AC/DC power networks more efficient to operate.

APPENDIX

Four-terminal AC/DC grid (100-MVA base power). - VSC units: $S_{nom} = 2$ p.u.; $\mathbf{z}_{ph1} = \mathbf{z}_{ph2} = \mathbf{z}_{ph3} = \mathbf{z}_{ph4} = 7.5\text{e-}4+ \text{j}0.075$ p.u.; $\mathbf{b}_f = \text{j}0.4$ p.u.; $\mathbf{z}_{34} = \mathbf{z}_{78} = \mathbf{z}_{11-12} = \mathbf{z}_{15-16} = 2.5\text{e-}3+\text{j}0.075$ p.u. - DC grid: $r_{12} = 0.00695$ p.u., $r_{13} = 0.010425$ p.u., $r_{24} = 0.0139$ p.u., $r_{34} = 0.017375$ p.u. - AC systems. AC 1: $\mathbf{z}_{12} = 0.02+\text{j}0.06$ p.u., $\mathbf{ys}_{12} = \text{j}0.06$ p.u.; $\mathbf{z}_{13} = 0.08+\text{j}0.24$ p.u., $\mathbf{ys}_{12} = \text{j}0.05$ p.u.; $\mathbf{z}_{23} = 0.06+\text{j}0.18$ p.u., $\mathbf{ys}_{23} = \text{j}0.04$ p.u; $P_{d3} = 2.5 + \text{j}0.5$ p.u. AC 2: $\mathbf{z}_{56} = 0.04+\text{j}0.12$ p.u., $\mathbf{ys}_{56} = \text{j}0.03$ p.u.; $\mathbf{z}_{57} = 0.04+\text{j}0.12$ p.u., $\mathbf{ys}_{57} = \text{j}0.03$ p.u.; $\mathbf{z}_{67} = 0.01+\text{j}0.03$ p.u., $\mathbf{ys}_{67} = \text{j}0.02$ p.u.; $P_{d7} = 2.0 + \text{j}0.5$ p.u. AC 3: $\mathbf{z}_{9-10} = 0.04+\text{j}0.12$ p.u., $\mathbf{ys}_{9-10} = \text{j}0.03$ p.u.; $\mathbf{z}_{9-11} = 0.04+\text{j}0.12$ p.u., $\mathbf{ys}_{9-11} = \text{j}0.03$ p.u.; $\mathbf{z}_{10-11} = 0.01+\text{j}0.03$ p.u., $\mathbf{ys}_{10-11} = \text{j}0.02$ p.u.; $P_{d11} = 2.0 + \text{j}0.5$ p.u. AC 4: $\mathbf{z}_{13-14} = 0.08+\text{j}0.24$ p.u., $\mathbf{ys}_{13-14} = \text{j}0.05$ p.u.; $\mathbf{z}_{13-15} = 0.06+\text{j}0.18$ p.u., $\mathbf{ys}_{13-15} = \text{j}0.04$ p.u.; $\mathbf{z}_{14-15} = 0.04+\text{j}0.12$ p.u., $\mathbf{ys}_{14-15} = \text{j}0.03$ p.u.; $P_{d13} = 0.5 + \text{j}0.1$ p.u.; $P_{d14} = 1.5 + \text{j}0.1$ p.u.; $P_{d15} = 0.5 + \text{j}0.1$ p.u.

Six-terminal AC/DC grid (100-MVA base power). - VSC units: $S_{nom} = 5$ p.u.; see Table 2. - DC grid: parameters taken from [25] and divided by S_{nom}. - AC 1 – AC 6: parameters taken from [25].

REFERENCES

[1] E. Acha, P. Roncero-Sanchez, A. De la Villa-Jaen, L. M. Castro, and B. Kazemtabrizi, *VSC-FACTS-HVDC: Analysis, Modelling and Simulation in Power Grids*. Hoboken, NJ, USA: Wiley, May 2019.

[2] W. Wang, G. Li, and J. Guo, "Large-scale renewable energy transmission by HVDC: Challenges and proposals," *Engineering*, vol. 19, pp. 252–267, Dec. 2022, doi: 10.1016/j.eng.2022.04.017.

[3] M. A. Hannan, S. B. Wali, P. J. Ker, M. S. A. Rahman, M. Mansor, V. K. Ramachandaramurthy, K. M. Muttaqi, T. M. I. Mahlia, and Z. Y. Dong, "Battery energy-storage system: A review of technologies, optimization objectives, constraints, approaches, and outstanding issues," *J. Energy Storage*, vol. 42, Oct. 2021, Art. no. 103023, doi: 10.1016/j.est.2021.103023.

[4] K. Prakash, M. Ali, M. N. I. Siddique, A. A. Chand, N. M. Kumar, D. Dong, and H. R. Pota, "A review of battery energy storage systems for ancillary services in distribution grids: Current status, challenges and future directions," *Frontiers Energy Res.*, vol. 10, p. 32, Sep. 2022, doi: 10.3389/fenrg.2022.971704.

[5] A. F. Ramos, I. Ahmad, D. Habibi, and T. S. Mahmoud, "Placement and sizing of utility-size battery energy storage systems to improve the stability of weak grids," *Int. J. Electr. Power Energy Syst.*, vol. 144, Jan. 2023, Art. no. 108427, doi: 10.1016/j.ijepes.2022.108427.

[6] H. Khajeh, C. Parthasarathy, E. Doroudchi, and H. Laaksonen, "Optimized siting and sizing of distribution-network-connected battery energy storage system providing flexibility services for system operators," *Energy*, vol. 285, Dec. 2023, Art. no. 129490, doi: 10.1016/j.energy.2023.129490.

[7] M. Ramírez, R. Castellanos, G. Calderón, and O. Malik, "Placement and sizing of battery energy storage for primary frequency control in an isolated section of the Mexican power system," *Electric Power Syst. Res.*, vol. 160, pp. 142–150, Jul. 2018, doi: 10.1016/j.epsr.2018.02.013.

[8] Y. Zhu, C. Liu, K. Sun, D. Shi, and Z. Wang, "Optimization of battery energy storage to improve power system oscillation damping," *IEEE Trans. Sustain. Energy*, vol. 10, no. 3, pp. 1015–1024, Jul. 2019, doi: 10.1109/TSTE.2018.2858262.

[9] F. Yao, T. K. Chau, X. Zhang, H. H. Iu, and T. Fernando, "An integrated transmission expansion and sectionalizing-based black start allocation of BESS planning strategy for enhanced power grid resilience," *IEEE Access*, vol. 8, pp. 148968–148979, 2020, doi: 10.1109/ACCESS.2020.3014341.

[10] L. M. Castro and D. R. Espinoza-Trejo, "Optimal placement of battery energy storage systems with energy time shift strategy in power networks with high penetration of photovoltaic plants," *Sustain. Energy, Grids Netw.*, vol. 35, Sep. 2023, Art. no. 101093, doi: 10.1016/j.segan.2023.101093.

[11] L. A. Wong, V. K. Ramachandaramurthy, S. L. Walker, and J. B. Ekanayake, "Optimal placement and sizing of battery energy storage system considering the duck curve phenomenon," *IEEE Access*, vol. 8, pp. 197236–197248, 2020, doi: 10.1109/ACCESS.2020.3034349.

[12] V. B. Pamshetti and S. P. Singh, "Coordinated allocation of BESS and SOP in high PV penetrated distribution network incorporating DR and CVR schemes," *IEEE Syst. J.*, vol. 16, no. 1, pp. 420–430, Mar. 2022, doi: 10.1109/JSYST.2020.3041013.

[13] H. Abdel-Mawgoud, S. Kamel, M. Khasanov, and T. Khurshaid, "A strategy for PV and BESS allocation considering uncertainty based on a modified Henry gas solubility optimizer," *Electric Power Syst. Res.*, vol. 191, Feb. 2021, Art. no. 106886, doi: 10.1016/j.epsr.2020.106886.

[14] M. Padhee, A. Pal, C. Mishra, and K. A. Vance, "A fixed-flexible BESS allocation scheme for transmission networks considering uncertainties," *IEEE Trans. Sustain. Energy*, vol. 11, no. 3, pp. 1883–1897, Jul. 2020, doi: 10.1109/TSTE.2019.2946133.

[15] A. Alzahrani, H. Alharthi, and M. Khalid, "Minimization of power losses through optimal battery placement in a distributed network with high penetration of photovoltaics," *Energies*, vol. 13, no. 1, p. 140, Dec. 2019, doi: 10.3390/en13010140.

[16] P. Lazzeroni and M. Repetto, "Optimal planning of battery systems for power losses reduction in distribution grids," *Electric Power Syst. Res.*, vol. 167, pp. 94–112, Feb. 2019, doi: 10.1016/j.epsr.2018.10.027.

[17] P. Boonluk, A. Siritaratiwat, P. Fuangfoo, and S. Khunkitti, "Optimal siting and sizing of battery energy storage systems for distribution network of distribution system operators," *Batteries*, vol. 6, no. 4, p. 56, Nov. 2020, doi: 10.3390/batteries6040056.

[18] P. Saini and L. Gidwani, "An environmental based techno-economic assessment for battery energy storage system allocation in distribution system using new node voltage deviation sensitivity approach," *Int. J. Electr. Power Energy Syst.*, vol. 128, Jun. 2021, Art. no. 106665, doi: 10.1016/j.ijepes.2020.106665.

[19] X. Su, Z. Zhang, Y. Liu, Y. Fu, F. Shahnia, C. Zhang, and Z. Y. Dong, "Sequential and comprehensive BESSs placement in unbalanced active distribution networks considering the impacts of BESS dual attributes on sensitivity," *IEEE Trans. Power Syst.*, vol. 36, no. 4, pp. 3453–3464, Jul. 2021, doi: 10.1109/TPWRS.2021.3051629.

[20] T. Wan, Y. Tao, J. Qiu, and S. Lai, "Data-driven hierarchical optimal allocation of battery energy storage system," *IEEE Trans. Sustain. Energy*, vol. 12, no. 4, pp. 2097–2109, Oct. 2021, doi: 10.1109/TSTE.2021.3080311.

[21] Y. Zheng, Y. Song, A. Huang, and D. J. Hill, "Hierarchical optimal allocation of battery energy storage systems for multiple services in distribution systems," *IEEE Trans. Sustain. Energy*, vol. 11, no. 3, pp. 1911–1921, Jul. 2020, doi: 10.1109/TSTE.2019.2946371.

[22] L. M. Castro, E. Acha, and J. R. Rodriguez-Rodriguez, "Efficient method for the real-time contingency analysis of meshed HVDC power grids fed by VSC stations," *IET Gener., Transmiss. Distrib.*, vol. 12, no. 13, pp. 3158–3166, Jul. 2018.

[23] A. J. Wood and B. F. Wollenberg, *Power Generation, Operation and Control*, 2nd ed. Hoboken, NJ, USA: Wiley, 1996.

[24] J. S. Guzmán-Feria, L. M. Castro, J. H. Tovar-Hernández, N. González-Cabrera, and G. Gutiérrez-Alcaraz, "Unit commitment for multi-terminal VSC-connected AC systems including BESS facilities with energy time-shifting strategy," *Int. J. Electr. Power Energy Syst.*, vol. 134, Jan. 2022, Art. no. 107367, doi: 10.1016/j.ijepes.2021.107367.

[25] C. Grigg, P. Wong, P. Albrecht, R. Allan, M. Bhavaraju, R. Billinton, Q. Chen, C. Fong, S. Haddad, S. Kuruganty, W. Li, R. Mukerji, D. Patton, N. Rau, D. Reppen, A. Schneider, M. Shahidehpour, and C. Singh, "The IEEE reliability test system-1996. A report prepared by the reliability test system task force of the application of probability methods subcommittee," *IEEE Trans. Power Syst.*, vol. 14, no. 3, pp. 1010–1020, Aug. 1999, doi: 10.1109/59.780914.

LUIS M. CASTRO received the bachelor's and master's degrees in electric power systems from Instituto Tecnológico de Morelia, in 2006 and 2008, respectively, the first Ph.D. degree from Universidad Michoacana de San Nicolás de Hidalgo (UMSNH), Morelia, Mexico, in 2013, and the second Ph.D. degree from Tampere University of Technology (TUT), Tampere, Finland, in 2016. He was with General Electric, Querétaro, Mexico, and has been an Energy Consultant to public and private electrical industries in Central America and South America. In 2015, he joined Universidad Nacional Autónoma de México (UNAM), where he is currently a full-time Professor with the Faculty of Engineering, Department of Electrical Energy. His research interests include the modeling, planning, and operation of AC/DC power networks with renewable energy sources and storage systems. He is an Active Member of the National Research System sponsored by Consejo Nacional de Humanidades, Ciencia y Tecnología (CONAHCyT), Mexico. He is part of the board of directors of the Federal Electricity Commission (CFE—Distribution), participating as an Independent Consultant.

● ● ●